Calpain activation is the major cause of cell death in photoreceptors expressing a rhodopsin misfolding mutation

Antonella Comitato[1], Davide Schiroli[1], Monica Montanari[1], Valeria Marigo[1,*]

[1]Department of Life Sciences, University of Modena and Reggio Emilia, via Campi, 287, 41125 Modena, Italy

[*]Corresponding Author: Valeria Marigo, Department of Life Sciences, University of Modena and Reggio Emilia, via Campi, 287, 41125 Modena, Italy; phone: +390592055392; fax: +390592055410; email: valeria.marigo@unimore.it

ORCID: 0000-0002-4428-2084

Abstract

The majority of mutations in rhodopsin (RHO) cause misfolding of the protein and has been linked to degeneration of photoreceptor cells in the retina. A lot of attention has been set on targeting ER-stress for the development of new therapies for inherited retinal degeneration caused by mutations in the *RHO* gene. Nevertheless, the cell death pathway activated by RHO misfolded protein is still debated. In this study, we analyzed the retina of the knock-in mouse expressing the P23H misfolded mutant RHO. We found persistent unfolded protein response (UPR) during degeneration. Interestingly, long-term stimulation of the PERK branch of ER-stress had a protective effect by phosphorylating nuclear factor erythroid 2-related factor 2 (NRF2) transcription factor, associated to antioxidant responses. Otherwise, we provide evidence that increased intracellular calcium and activation of calpains strongly correlated with rod photoreceptor cell death. By blocking calpain activity we significantly decreased activation of caspase-7 and apoptosis inducing factor (AIF), two cell death effectors, as well as cell demise and effectively protected the retina from degeneration caused by the P23H dominant mutation in RHO.

Keywords

adRP, rod, eIF2α, spectrin, PD150606, Z-VAD-FMK, GSK2606414A

Introduction

Inherited retinal dystrophies, such as Retinitis Pigmentosa (RP), are major causes of blindness characterized by the progressive loss of photoreceptor cells. Mutations in the *Rhodopsin* (*RHO*) gene are linked to retinal dystrophy. The vast majority of these mutations have an autosomal dominant trait of inheritance and account for 25% of patients with adRP [1]. RHO is a G-protein coupled receptor activated by light in the phototransduction cascade of rod photoreceptors. RHO consists of a protein moiety (opsin) covalently bound to the chromophore (11-*cis*-retinal). Light induces the *cis* to *trans* isomerization of 11-*cis*-retinal and triggers the phototransduction cascade. The molecular mechanisms underlying cell death caused by dominant mutations in RHO are still not well characterized. The substitution of proline 23 to histidine (P23H) is the most common mutation in USA among hundreds of mutations in RHO identified so far and it is the most studied one [2]. This mutation most likely leads to misfolding of the protein and endoplasmic reticulum (ER) retention [3–5]. The quality control imposed by the ER activates three signal transduction cascades termed the unfolded protein response (UPR) to allow only properly folded proteins to leave the ER, whereas unfolded proteins are degraded. In case a cell cannot cope with UPR, it will be eliminated by apoptosis. The transducers of the UPR are three ER transmembrane proteins: the inositol-requiring enzyme 1 (IRE1), the activating transcription factor-6 (ATF6) and the protein kinase R-like ER protein kinase (PERK). In ER-stress caused by protein misfolding the early responses are set in motion via IRE1 that quickly attenuates if the stress persists; the ATF6 responses are also diminished with time but with slower kinetics. By contrast, the responses mediated by PERK can persist under prolonged ER-stress. Persistent IRE1 signaling was associated to enhanced cell survival while constant PERK activation was coupled to apoptosis in several cell types and in photoreceptors [6]. The response to misfolded proteins is set in motion by IRE1 and PERK phosphorylation and activation. IRE1

is a ribonuclease that splices the mRNA encoding X-box transcription factor 1 (*Xbp1*), generating a transcription activator that increases the expression of chaperones (i.e. *Gpr78*/*Bip*/*Hsp5*), favoring protein folding. PERK phosphorylates eukaryotic initiation factor-2α (eIF2α) resulting in the reduction of protein synthesis and the up-regulation of ATF4 that promotes the expression of several genes such as growth arrest and the transcription factor DNA-damage-inducible protein 153 (*Gadd153/Chop*) [7].

ER-retention of the misfolded protein and ER-stress have been correlated to cell death in two murine models of RP caused by dominant mutations in RHO [4,6,8,9]. This cell death mechanism was targeted in newly developed therapeutic approaches based on ER-stress inhibition or pharmacological chaperone delivery [4,10–13]. Besides ER-stress sensors, we showed that photoreceptors expressing high levels of P23H mutant RHO (Rho^{TgP23H} and $Rho^{P23H/-}$) also suffer increased intracellular calcium and activation of calpain proteases leading to nuclear translocation of the apoptosis inducing factor (AIF) and chromatin fragmentation [14].

At the moment, the knock-in mouse bearing the P23H mutation in RHO ($Rho^{P23H/+}$) is considered the best model of the disease with a slow progression of photoreceptor degeneration starting from the inferior retina, similarly to what has been reported in patients [15]. Specifically, degradation of the mutated RHO protein through the ER-associated protein degradation (ERAD) pathway as well as rod outer segment structural defects were reported in this knock-in model [15–17]. The study of the pathophysiologic effects of ER-stress in $Rho^{P23H/+}$ mutant photoreceptors demonstrated persistent activation of the UPR sensor IRE1 up to 88 days after birth (PN88) without upregulation of *Gadd153/Chop* expression [17].

We and other suggested several novel treatments to target dominant mutations in RHO [13,14,18–22]. The published studies showed incomplete rescue of the phenotype possibly

due to the limited understanding of the molecular mechanisms underlying cell death in photoreceptors expressing misfolded RHO.

In this study, we molecularly evaluated the different contribution of ER-stress and calcium unbalance in retinal degeneration in the *Rho*$^{P23H/+}$ mouse model. We demonstrate sustained activation of the IRE1 and PERK branches of the UPR during the progression of the disease in the *Rho*$^{P23H/+}$ retina. We propose that both these pathways are possibly involved in the degradation of misfolded P23H mutant RHO and in counteracting the toxic effects of the mutation. We also show that PERK accomplishes this function through activation of the nuclear factor erythroid 2-related factor 2 (NRF2) transcription factor. On the other hand, we provide evidence that activation of calpain proteases by increased intracellular calcium ions is the major cause of cell death.

Material and Methods

Animal care and treatments

All procedures on mice were conducted at CSSI (Centro Servizi Stabulario Interdipartimentale), approved by the Ethical Committee of University of Modena and Reggio Emilia and by the Italian Ministero della Salute (346/2015-PR) and were in accordance with the ARVO Statement for the Use of Animals in Ophthalmic and Vision Research. *Rho*$^{P23H/+}$ mice, on a C57BL/6J background, were maintained in 12hr light/dark cycles and had free access to food and water. For intravitreal administration, mice at PN18 were anesthetized with an intraperitoneal injection of 250 mg/kg body weight of avertin (1.25% (w/v) 2,2,2-tribromoethanol and 2.5% (v/v) 2-methyl-2-butanol; Sigma). Subsequently, eyes were intravitreously injected via a trans-scleral trans-choroidal approach with 0.5 μl of PD150606 pan-calpain inhibitor (1.5mM solution with an expected final concentration in the eye of 150 μM; Sigma) or Z-VAD-FMK pan-caspase inhibitor (25 ng/eye; Sigma) or GSK2606414A PERK inhibitor (100 μM solution with an expected final concentration in the eye of 10 μM; GSK). Control eyes received vehicle only. Mice treated with different compounds were sacrificed 16 hours later, at PN19.

Cytofluorimetric analysis of calcium

Intracellular calcium levels were determined with the calcium probe Fluo-4 AM (Life Technologies), as previously published [14,23]. Briefly, wild type and *Rho*$^{P23H/+}$ retinas at PN19 were harvested and incubated with 19 U/ml of papain for 30 min and, after 33-fold dilution with DMEM containing 10 U/ml DNAse, retina cells were dissociated by trituration. After three washes with PBS, cells were incubated with 1 μM Fluo-4 AM at 37°C for 30 min in Ca^{2+}-free medium. Photoreceptor cells were characterized by staining with anti-Rho antibody 1D4 (1:1000, Sigma) and with anti-Recoverin (1:500, Millipore), as in [14,23], and

plotted over the forward scatter to define the gating strategy for the following intracellular calcium analysis. Retinal cells from four wild type and four *Rho*$^{P23H/+}$ mice, derived from at least three different litters, were gated. Fluorescence was measured in 20,000 events with a Coulter Epics XL-MCL flow cytometer (Beckman Coulter) at an excitation wavelength of 488 nm. Fluo-4 AM median fluorescence intensity (MFI) was measured in cells from each dissociated *Rho*$^{P23H/+}$ retina and compared to MFI from wild type photoreceptors from littermates.

Calpain activity assay

Cryosections from unfixed retinas were incubated for 15 min in calpain reaction buffer (CRB: 25 mM HEPES-KOH pH 7.2, 65 mM KCl, 2 mM $MgCl_2$, 1.5 mM $CaCl_2$, 2 mM DTT), as previously described [14], and then exposed for 1 h at 37°C to the fluorescent calpain substrate CMAC, t-BOC-Leu-Met (A6520; Invitrogen) at a final concentration of 2 µM. Slides were washed twice for 10 min each in CRB, mounted with mowiol 4-88 (Sigma) and analyzed at a Zeiss Axio Imager A2 microscope using the filter excitation/emission 365/420. Labeled cells were counted in the outer nuclear layer (ONL), which contains photoreceptors, in at least three entire sections, with a dorsal-ventral orientation, passing through the optic nerve from three independent experiments. Specificity of the assay was demonstrated by omitting the CMAC, t-BOC-Leu-Met substrate or by pretreatment of the crysections with calpain inhibitor (Fig. S1a).

DNA Nick-End Labeling by TUNEL and immunofluorescence

Eyes were oriented, fixed in Davidson's fixative (8% Formaldehyde, 31.5% Ethanol, 2 M Acetic Acid), embedded in paraffin and sectioned. Apoptotic nuclei were detected by TdT-mediated dUTP terminal nick-end labelling kit (TUNEL, fluorescein; Roche) according to the

producer's protocols. Primary antibodies were used as follows: anti-AIF (1:100; Sigma), anti-phosphorylated-IRE1 (1:200; Novus Biologicals), anti-phosphorylated-PERK (1:100; Cell Signaling). Secondary antibodies were Alexa Fluor® 568 anti-mouse and anti-rabbit antibodies (1:1000; Molecular Probes). Nuclei were stained with 4′,6-diamidino-2-phenylindole (DAPI). Slides were mounted with mowiol 4-88 (Sigma) and analyzed at a Zeiss Axio Imager A2 microscope. Quantification of dying cells was performed by counting all TUNEL labeled cells in the photoreceptor cell layer in at least three entire retinal sections, with a dorsal-ventral orientation, passing through the optic nerve derived from different animals. The number of photoreceptors double labelled with anti-AIF and TUNEL was counted by staining of nuclei with DAPI and was used to calculate percentages of dying cells, as previously published [23].

Retinal protein extracts and western blotting analysis

Retinas were lysed as previously described to obtain nuclear-enriched proteins and total cellular proteins [24]. The purity of enriched lysates was checked by immunoblotting using a nuclear marker (anti-Histone H3 1:3000; Bethyl Laboratories) or a cytosol marker (anti-pan-actin, 1:3000; Millipore). Equivalent amounts of protein extracts (20 μg) were resolved using SDS-PAGE and immunoblottings were performed following standard procedures. The antibodies used for western blotting were: anti-αII-spectrin (AA6, 1:2000; Enzo Life) [25], anti-AIF (1: 1000; Calbiochem) [26], anti-Caspase7 (1:1000; Cell Signaling), anti-eIF2α (1:1000; Cell Signaling), anti-NRF2 (1:2000; Invitrogen), anti-phosphorylated-IRE1 (1:2000; Novus Biologicals), anti-phosphorylated-PERK (1:1000; Cell Signaling), anti-phosphorylated-eIF2α (1:1000; Cell Signaling). Antibodies specificity is shown in Fig. S2. Each blot analyzed proteins derived from 4 retinas pooled together and 3 independent pools

from 3 different litters were used as biological replicates, one representative blot is shown. The entire blots are shown in Fig. S3.

Statistical analysis

Cell count analyses are shown as mean ± SD. Student's t-test analysis was performed to compare data derived from at least three different mock treated mutant retinas to at least three different contralateral mutant retinas treated with different compounds. ANOVA test was performed to compare data from retinas at different ages or after different treatments.

Results

P23H mutation causes increased intracellular calcium and activation of calpains

We previously demonstrated increased intracellular Ca^{2+} in transgenic mice expressing only the P23H mutant RHO, in the absence of wild type RHO, and in the *Rho* knock-out retina [14]. In the present study, we focused on a more relevant model in which P23H mutant RHO is in heterozygosity with wild type RHO, a genotype similar to the human condition. We characterized photoreceptor cell death in the $Rho^{P23H/+}$ retinas by TUNEL assay, as previously published [14], and found a peak at 19 days after birth (PN19) (Fig. 1a). Retinas older than PN31 showed very few $TUNEL^{+}$ cells in each analyzed section, indicating that starting from the age of 1 month a slow and constant cell death led to the gradual progression of photoreceptor degeneration in this mouse model of adRP. We focused our molecular analyses at PN19, the time point with the highest number of cells undergoing cell death. We started by evaluating intracellular Ca^{2+} by flow cytometry and found it statistically increased in $Rho^{P23H/+}$ photoreceptors (Fig. 1b), similarly to what we previously found in other models with mutations in RHO [14]. Increased intracellular Ca^{2+} can induce activation of calpain proteases, cell death initiators in several forms of RP [14,24,26–28]. Based on

the link between high intracellular Ca^{2+} and calpains, we assessed calpain activation by an *in situ* enzymatic assay and by cleavage analysis of αII-spectrin, a known substrate of calpain proteases. Both assays confirmed activation of calpain proteases in *Rho*$^{P23H/+}$ retinas (Fig. 1c-d). Co-labelling of TUNEL and the *in situ* calpain activity assay defined that calpain activation occurred in 80-90% of photoreceptor cells undergoing cell death at all ages analyzed (Fig. 1c and Fig. S1b). Different molecular weight fragments of αII-spectrin are generated upon cleavage by calpains (150 kDa and 145 kDa) or by caspases (150 kDa and 120 kDa) [29]. The immunoblot on protein extracts from wild type and *Rho*$^{P23H/+}$ revealed an increase of fragments with molecular weights consistent with calpain and caspase activations (Fig. 1d).

The cell death effector in photoreceptors triggered by calpains is AIF [14,24,26], a factor that, upon cleavage by calpains, translocates from mitochondria to the nucleus where, together with EndoG, promotes chromatin condensation and fragmentation [30,31]. Western blotting of nuclear extracts confirmed nuclear translocation of AIF in the *Rho*$^{P23H/+}$ retina at PN19 (Fig. 1e). Immunolocalization defined that AIF was present in nuclei of most photoreceptor cells undergoing cell death, as defined by TUNEL (Fig. 1f, arrows).

Altogether these data suggested that *Rho*$^{P23H/+}$ mutant rod photoreceptors activate a cell death mechanism engaging calpains and AIF.

Activation of ER stress sensors during retinal degeneration

The P23H RHO mutation was previously reported by us and others as a mutation that causes protein misfolding and ER retention [3,4,14,17,32–34]. We thus assessed activation of the ER sensor proteins by western blotting and immunofluorescence. We detected phosphorylation of IRE1 and PERK and both sensors are maintained phosphorylated and activated at least up to PN60. Immunofluorescence studies showed that activation of both

sensors happened in photoreceptor cells. (Fig. 2a-b). Activation of the PERK pathways was confirmed at all analyzed time points by detection of phosphorylated eIF2α, its direct target (Fig. 2a). The PERK pathway can lead to apoptosis by activating caspases. We thus checked cleavage of caspase-7, an effector caspase previously linked to cell death in photoreceptors expressing mutant RHO [4,35]. The cleaved activated caspase-7 was detected in *Rho*$^{P23H/+}$ retinas at PN19 and PN60 (Fig. 2c).

The PERK pathway can also phosphorylate and stabilize the transcription factor NRF2 leading to its translocation to the nucleus. NRF2 has been reported, in other cell systems, to be requested for survival during UPR by promoting redox homeostasis upon induction of ER sensors [36,37]. Interestingly, we observed higher levels of phosphorylated NRF2 in nuclear extracts from *Rho*$^{P23H/+}$ retinas compared to age matched wild type retinas (Fig. 2d). The amount of phosphorylated NRF2 increased with age and was found more abundant in PN60 retinal cell nuclei than in younger retinas.

The analyses of ER sensors pathways indicated that the P23H RHO mutation, when expressed in heterozygosity with the wild type allele, triggered the UPR, a response maintained during degeneration. Interestingly, ER sensor activation did not correlate with the changes in cell death observed by TUNEL assay. In fact, TUNEL labeled cells decreased after a peak at PN19, but IRE1 and PERK phosphorylations were well detected at both ages and did not decrease with degeneration progression.

PERK sustains UPR

Based on the finding that *Rho*$^{P23H/+}$ photoreceptors turn on IRE-1 and PERK and that we detect a cell death mechanism linked to caspase-7 together with the NRF2 survival response, we wondered whether the PERK branch of the UPR was associated with cell death or survival in this murine model of retinal dystrophy. To address this question we

treated *Rho*$^{P23H/+}$ mice with a validated PERK inhibitor, GSK2606414A [38]. This inhibitor has been previously demonstrated to block the PERK branch and reduce eIF2α phosphorylation in P23H transgenic rat retinas. We intravitreally injected the PERK inhibitor in PN18 retinas and the effects were evaluated 16 hours later, at PN19. Upon treatments with GSK2606414A, we detected a reduction of eIF2α phosphorylation, which demonstrates that the PERK inhibitor was effective (Fig. 3a). Similarly to what previously reported in the rat model expressing P23H RHO, we correlated inhibition of PERK with a significant increase of photoreceptor cell death (Fig. 3b and Fig. S4). To molecularly characterize the mechanism underlying the increase of cell death we evaluated the two targets of PERK, i.e. NRF2 and caspase-7. Inhibition of PERK caused a reduction of phosphorylation and nuclear translocation of NRF2 (Fig. 3c). Otherwise, blocking the PERK pathway did not affect caspase-7 that was maintained activated (Fig. 3d).

Altogether, data from retinas treated with the PERK inhibitor suggested that the PERK pathway was activated upon expression of P23H mutant RHO, however PERK fulfilled a role of protection from cell death by activating NRF2 in photoreceptor cells. It appeared that PERK did not participate to the activation of caspase-7.

Calpains play a major role in photoreceptor cell death

Activation of calpains has been reported in several models of retinal degeneration [14,24,26–28] and calpains can cleave caspase-7 generating p17/p18 active fragments [39]. We, thus, hypothesized that activation of caspase-7 in the *Rho*$^{P23H/+}$ mutant retina could be triggered by calpains. To address this hypothesis we intravitreally injected a pan-calpain inhibitor (PD150606) previously reported to block calpains in transgenic rats expressing the S334ter mutant RHO [20]. Histology of injected eyes is shown in Fig S5. PD150606 reduced calpain activation *in vivo* in the *Rho*$^{P23H/+}$ retina by about 65%, as also demonstrated by the

strong decrease of 145-150 kDa and 120 kDa cleaved αII-spectrin (Fig. 4a-b). The calpain inhibitor was very effective in protecting the retina from cell death with a significant reduction of almost 70% of TUNEL^{+} cells (Fig. 4c and Fig. S4). Remarkably, inhibition of calpains caused a strong reduction of the p17 activated caspase-7 fragment (Fig. 4d).

To define the contribution of caspase-7 to photoreceptor cell death in *Rho*$^{P23H/+}$ mice, we intravitreally injected the pan-caspase inhibitor, Z-VAD-FMK. Z-VAD-FMK interfered with caspase-7 activation (Fig. 4d) and strongly reduced the 120 kDa αII-spectrin fragment derived from caspase cleavage (Fig. 4b, arrow) but did not affect the 145-150 kDa αII-spectrin fragments derived from calpain cleavage (Fig. 4b, asterisk). Inhibition of caspase-7 significantly reduced cell death of 34% (Fig. 4c and Fig. S4) and partially decreased calpain activity of about 5%. Co-treatment with calpain and caspase inhibitors significantly protected the *Rho*$^{P23H/+}$ mutant retina from cell death but the effect did not appear to be additive. We observed reductions of calpain activation and cell death similar to what found by the singular treatment with calpain inhibitor (Fig. 4a and 4c).

These results imply that photoreceptor cell death is mainly mediated by calpain activation in the *Rho*$^{P23H/+}$ mutant retina and that caspase-7 activation is triggered by calpains and not by ER-stress.

Discussion

Common forms of retinal degeneration are associated to mutations in the *RHO* gene. Several studies characterized the effects of the amino acid changes on the RHO protein and proposed different classifications of the mutations based on the analyzed parameters [3,40–42]. These studies reported a high percentage of mutations in RHO that affect protein structure and stability. RHO accounts for approximately 30% of the rod photoreceptor proteome [43]. Misfolding mutations in RHO, such as P23H and T17M, have thus a strong impact on the photoreceptor cell homeostasis and have been demonstrated to activate UPR, ER-associated degradation (ERAD) pathways and ER-stress responses [8,14,17,33]. Attempts have been made in the last years to protect photoreceptors from cell death caused by dominant mutations in RHO by targeting these pathways [4,44]. Nevertheless, none of these therapeutic strategies could rescue the degeneration phenotype, possibly because protein misfolding can trigger UPR and ER-stress, two pathways that are partially overlapping and activate shared ER sensors [6].

New evidences implied that cell death caused by mutant RHO might be initiated by alternative pathways not involving the ER sensors. In fact, in the relevant *Rho*$^{P23H/+}$ mouse model the IRE1 ER sensor, which is supposed to induce a response aimed at relieving the cell from protein misfolding, is sustained in rod photoreceptors at ages when degeneration progresses [17]. Secondly, inhibition of the PERK pathway could aggravate degeneration caused by expression of P23H RHO in a transgenic rat model [38]. In the rat model activation of necroptosis had also been detected [45].

The molecular mechanism causing cell death in photoreceptors expressing misfolded RHO was, thus, not well understood and required further characterization, which was necessary for the development of appropriate therapeutic strategies. In the present study, we report that the knock-in *Rho*$^{P23H/+}$ mouse shows a peak of cell death a PN19 and that degeneration

slowly continues at later ages. The timing of the peak of cell death corresponds with terminal development of the rod outer segment, previously reported to happen between PN11 and PN24 [46], and with the recorded dark current, which increases proportionally with outer segment formation [47]. The instability of P23H mutant RHO [48] may accelerate degeneration at early stages of rod differentiation when the rod photoreceptors are still undergoing maturation. We also demonstrate during the degeneration process persistent activation of two ER sensors previously described to mediate opposite effects: IRE1, a compensatory response, and PERK, a response leading to cell death [6]. Our data agree with the previously reported maintenance of IRE1 signaling during degeneration caused by P23H RHO [17], but we also detected continuous activation of PERK, as defined by PERK and EIF-2α phosphorylation. This discrepancy may be due to the different murine ages analyzed. Nevertheless, we concur that activation of ER sensors and UPR are not the leading cause of photoreceptor cell death but, possibly, a pathophysiologic effect triggering survival responses. This assumption is based on our identification of NRF2 as a putative mediator of the PERK compensatory response. This is founded on our data showing that phosphorylated nuclear NRF2 levels decreased upon exposure of the retina to an inhibitor of PERK and that this treatment was detrimental for the degenerating retina. NRF2 is a transcription factor that binds to the antioxidant response element (ARE) and regulates over 250 genes in the antioxidant cell response [49]. The correlation of NRF2 nuclear reduction with increased cell death following the PERK inhibitor treatment and the previously demonstrated role of NRF2 as a neuroprotective agent in retinal degeneration [50–53], implied that photoreceptors activate a remedial mechanism to alleviate stress derived from misfolding of RHO in the ER. Interference with this mechanism accelerated degeneration, as found in the treatments with PERK inhibitor. The relevance of NRF2 pathway as a neuroprotective mechanism is also supported by the observation of some preservation of

the retina after treatments of rabbits expressing a dominant mutation in RHO with a NRF2 activator [54]. A second compensatory mechanism activated by the UPR may lead to the reduction of P23H RHO levels in the *Rho*$^{P23H/+}$ mouse model [15], which may also rely on PERK activation, as demonstrated in an *in vitro* study on several RHO mutations [55].

The ER operates as an intracellular Ca^{2+} storage organelle and elevation of $[Ca^{2+}]_i$ is a well-documented feature of ER-stress and cell death [56]. Increases of $[Ca^{2+}]_i$ can trigger calpains, proteases acting on several substrates, and among those on AIF, and leading photoreceptor cells to degeneration [26]. Increased levels of Ca^{2+} and activation of calpains are common features in retinal degeneration caused by mutations in different genes and several calpain inhibitors demonstrated to be effective to restrain photoreceptor degeneration [26,27,57–61]. The studies in the *Rho*$^{P23H/+}$ mouse model of retinal degeneration confirmed the calcium-calpain pathway as a common mechanism activated by photoreceptor demise even at later stages of degeneration. This is an important point because patients usually refer to the ophthalmologist when the disease is at an advanced stage. Safety of long-term treatments and development of appropriate delivery systems for calpain inhibitors need to be evaluated to transfer this finding to patients.

In the P23H transgenic rat model treatments with a calpain inhibitor had a much lower neuroprotective effect compared to those observed with our treatments [45]. This discrepancy may be due to i) the use of a different calpain inhibitor, calpeptin, that targets calpain 1, calpain 2 and the permeability transition pore. PD150606 is more specific for calpains and inhibits several calpains, not only calpain 1 and calpain 2, by binding to the calcium binding domain; ii) the different administration protocol of the drug; iii) the different animal model.

In summary, a good comprehension of the molecular pathways activated during photoreceptor degeneration caused by protein misfolding is fundamental for a targeted

design of new therapeutic approaches for several forms of retinal dystrophy in which protein homeostasis is deregulated, not only caused by mutations in RHO [62]. Here we identified the calcium-calpain pathway as the major cause of photoreceptor demise in the $Rho^{P23H/+}$ mutant retina and defined it as a target in several forms of retinal dystrophy.

Notes

Acknowledgements

The authors acknowledge the Cell-lab Facility and CSSI of University of Modena and Reggio Emilia for cytofluorimetric analysis and animal husbandry assistance.

Author Contributions

A.C. and D.S. performed experimental procedures and contributed to the writing of the manuscript. M.M. performed flow cytometry analysis. V.M designed and supervised the experiments and wrote the manuscript.

Informed consent

Informed consent was obtained from all individual participants included in the study.

Funding Information

V.M. was supported by research grant Fondazione Roma grant (call for proposals 2013 on Retinitis Pigmentosa), European Union (transMed, MSCA-ITN-2017-765441) and Fondazione Telethon (grant numbers GGP11210, GGP14180).

Compliance with Ethical Standards

All procedures on mice were conducted at CSSI (Centro Servizi Stabulario Interdipartimentale), approved by the Ethical Committee of University of Modena and Reggio Emilia and by the Italian Ministero della Salute (346/2015-PR) and were in accordance with the ARVO Statement for the Use of Animals in Ophthalmic and Vision Research.

Conflict of Interest

The authors declare that they have no conflict of interest.

References

1. Hartong DT, Berson EL, Dryja TP. Retinitis pigmentosa. Lancet. 2006;368:1795–809.

2. Dryja TP, McGee TL, Reichel E, Hahn LB, Cowley GS, Yandell DW, et al. A point mutation of the rhodopsin gene in one form of retinitis pigmentosa. Nature. 1990;343:364–366.

3. Behnen P, Felline A, Comitato A, Di Salvo MT, Raimondi F, Gulati S, et al. A Small Chaperone Improves Folding and Routing of Rhodopsin Mutants Linked to Inherited Blindness. iScience. 2018;4:1–19.

4. Gorbatyuk MS, Knox T, LaVail MM, Gorbatyuk OS, Noorwez SM, Hauswirth WW, et al. Restoration of visual function in P23H rhodopsin transgenic rats by gene delivery of BiP/Grp78. Proc Natl Acad Sci USA. 2010;107:5961–5966.

5. Price BA, Sandoval IM, Chan F, Simons DL, Wu SM, Wensel TG, et al. Mislocalization and Degradation of Human P23H-Rhodopsin-GFP in a Knockin Mouse Model of Retinitis Pigmentosa. Invest Ophthalmol Vis Sci. 2011;52:9728–9736.

6. Lin JH, Li H, Yasumura D, Cohen HR, Zhang C, Panning B, et al. IRE1 signaling affects cell fate during the unfolded protein response. Science. 2007;318:944–949.

7. McCullough KD, Martindale JL, Klotz L-O, Aw T-Y, Holbrook NJ. Gadd153 sensitizes cells to endoplasmic reticulum stress by down-regulating Bcl2 and perturbing the cellular redox state. Mol Cell Biol. 2001;21:1249–1259.

8. Kunte MM, Choudhury S, Manheim JF, Shinde VM, Miura M, Chiodo VA, et al. ER Stress Is Involved in T17M Rhodopsin-Induced Retinal Degeneration. Invest Ophthalmol Vis Sci. 2012;53:3792–3800.

9. Kroeger H, Messah C, Ahern K, Gee J, Joseph V, Matthes MT, et al. Induction of Endoplasmic Reticulum Stress Genes, BiP and Chop, in Genetic and Environmental Models of Retinal Degeneration. Invest Ophthalmol Vis Sci. 2012;53:7590–7599.

10. Ohgane K, Dodo K, Hashimoto Y. Retinobenzaldehydes as proper-trafficking inducers of folding-defective P23H rhodopsin mutant responsible for retinitis pigmentosa. Bioorg Med Chem. 2010;18:7022–7028.

11. Athanasiou D, Bevilacqua D, Aguila M, McCulley C, Kanuga N, Iwawaki T, et al. The co-chaperone and reductase ERdj5 facilitates rod opsin biogenesis and quality control. Hum Mol Genet. 2014;23:6594–6606.

12. Chen Y, Chen Y, Jastrzebska B, Golczak M, Gulati S, Tang H, et al. A novel small molecule chaperone of rod opsin and its potential therapy for retinal degeneration. Nat Comm. 2018;9:1976.

13. Mendes HF, Zaccarini R, Cheetham ME. Pharmacological manipulation of rhodopsin retinitis pigmentosa. Adv Exp Med Biol. 2010;664:317–323.

14. Comitato A, Di Salvo MT, Turchiano G, Montanari M, Sakami S, Palczewski K, et al. Dominant and recessive mutations in rhodopsin activate different cell death pathways. Hum Mol Genet. 2016;25:2801–2812.

15. Sakami S, Maeda T, Bereta G, Okano K, Golczak M, Sumaroka A, et al. Probing mechanisms of photoreceptor degeneration in a new mouse model of the common form of autosomal dominant retinitis pigmentosa due to P23H opsin mutations. J Biol Chem. 2011;286:10551–10567.

16. Sakami S, Kolesnikov A V, Kefalov VJ, Palczewski K. P23H opsin knock-in mice reveal a novel step in retinal rod disc morphogenesis. Hum Mol Genet. 2014;23:1723–1741.

17. Chiang W-C, Kroeger H, Sakami S, Messah C, Yasumura D, Matthes MT, et al. Robust Endoplasmic Reticulum-Associated Degradation of Rhodopsin Precedes Retinal Degeneration. Mol Neurobiol. 2015;52:679–695.

18. Botta S, Marrocco E, de Prisco N, Curion F, Renda M, Sofia M, et al. Rhodopsin targeted

transcriptional silencing by DNA-binding. Elife. 2016;5:e12242.

19. Griciuc A, Aron L, Ueffing M. ER stress in retinal degeneration: a target for rational therapy? Trends Mol Med. 2011;17:442–451.

20. Ozaki T, Ishiguro S, Hirano S, Baba A, Yamashita T, Tomita H, et al. Inhibitory peptide of mitochondrial μ-calpain protects against photoreceptor degeneration in rhodopsin transgenic S334ter and P23H rats. PLoS One. 2013;8:e71650.

21. Latella MC, Di Salvo MT, Cocchiarella F, Benati D, Grisendi G, Comitato A, et al. In vivo editing of the human mutant Rhodopsin gene by electroporation of plasmid-based CRISPR/Cas9 in the mouse retina. Mol Ther Nucleic Acids. 2016;5:e389.

22. Mussolino C, Sanges D, Marrocco E, Bonetti C, Di Vicino U, Marigo V, et al. Zinc-finger-based transcriptional repression of rhodopsin in a model of dominant retinitis pigmentosa. EMBO Mol Med. 2011;3:118–128.

23. Comitato A, Subramanian P, Turchiano G, Montanari M, Becerra SP, Marigo V. Pigment epithelium-derived factor hinders photoreceptor cell death by reducing intracellular calcium in the degenerating retina. Cell Death Dis. 2018;9:560.

24. Comitato A, Sanges D, Rossi A, Humphries MM, Marigo V. Activation of Bax in Three Models of Retinitis Pigmentosa. Invest Ophthalmol Vis Sci. 2014;55:3555–3562.

25. Doonan F, Donovan M, Cotter TG. Activation of Multiple Pathways during Photoreceptor Apoptosis in the rd Mouse. Invest Ophthalmol Vis Sci. 2005;46:3530–3538.

26. Sanges D, Comitato A, Tammaro R, Marigo V. Apoptosis in retinal degeneration involves cross-talk between apoptosis-inducing factor (AIF) and caspase-12 and is blocked by calpain inhibitors. Proc Natl Acad Sci USA. 2006;103:17366–17371.

27. Arango-Gonzalez B, Trifunović D, Sahaboglu A, Kranz K, Michalakis S, Farinelli P, et al. Identification of a common non-apoptotic cell death mechanism in hereditary retinal

degeneration. PLoS One. 2014;9:e112142.

28. Paquet-Durand F, Azadi S, Hauck SM, Ueffing M, van Veen T, Ekström P. Calpain is activated in degenerating photoreceptors in the rd1 mouse. J Neurochem. 2006;96:802–814.

29. Pike BR, Flint J, Dave JR, Lu X-CM, Wang KKK, Tortella FC, et al. Accumulation of Calpain and Caspase-3 Proteolytic Fragments of Brain-Derived αII-Spectrin in Cerebral Spinal Fluid after Middle Cerebral Artery Occlusion in Rats. J Cereb Blood Flow Metab. 2004;24:98–106.

30. Arnoult D, Gaume B, Karbowski M, Sharpe JC, Cecconi F, Youle RJ. Mitochondrial release of AIF and EndoG requires caspase activation downstream of Bax/Bak-mediated permeabilization. Embo J. 2003;22:4385–4399.

31. Polster BM, Basanez G, Etxebarria A, Hardwick JM, Nicholls DG. Calpain I induces cleavage and release of apoptosis-inducing factor from isolated mitochondria. J Biol Chem. 2005;280:6447–6454.

32. Frederick JM, Krasnoperova N V, Hoffmann K, Church-Kopish J, Ruther K, Howes K, et al. Mutant rhodopsin transgene expression on a null background. Invest Ophthalmol Vis Sci. 2001;42:826–833.

33. Griciuc A, Aron L, Piccoli G, Ueffing M. Clearance of Rhodopsin(P23H) aggregates requires the ERAD effector VCP. Biochim Biophys Acta. 2010;1803:424–434.

34. Kroeger H, Chiang WC, Lin JH. Endoplasmic reticulum-associated degradation (ERAD) of misfolded glycoproteins and mutant P23H rhodopsin in photoreceptor cells. Adv Exp Med Biol. 2012;723:559–565.

35. Choudhury S, Bhootada Y, Gorbatyuk O, Gorbatyuk M. Caspase-7 ablation modulates UPR, reprograms TRAF2-JNK apoptosis and protects T17M rhodopsin mice from severe

retinal degeneration. Cell Death Dis. 2013;4:e528–e528.

36. Cullinan SB, Zhang D, Hannink M, Arvisais E, Kaufman RJ, Diehl JA. Nrf2 is a direct PERK substrate and effector of PERK-dependent cell survival. Mol Cell Biol. 2003;23:7198–7209.

37. Cullinan SB, Diehl JA. PERK-dependent activation of Nrf2 contributes to redox homeostasis and cell survival following endoplasmic reticulum stress. J Biol Chem. 2004;279:20108–20117.

38. Athanasiou D, Aguila M, Bellingham J, Kanuga N, Adamson P, Cheetham ME. The role of the ER stress-response protein PERK in rhodopsin retinitis pigmentosa. Hum Mol Genet. 2017;26:4896–4905.

39. Gafni J, Cong X, Chen SF, Gibson BW, Ellerby LM. Calpain-1 Cleaves and Activates Caspase-7. J Biol Chem. 2009;284:25441–25449.

40. Athanasiou D, Aguila M, Bellingham J, Li W, McCulley C, Reeves PJ, et al. The molecular and cellular basis of rhodopsin retinitis pigmentosa reveals potential strategies for therapy. Prog Retin Eye Res. 2018;62:1–23.

41. Briscoe AD, Gaur C, Kumar S. The spectrum of human rhodopsin disease mutations through the lens of interspecific variation. Gene. 2004;332:107–118.

42. Krebs MP, Holden DC, Joshi P, Clark III CL, Lee AH, Kaushal S. Molecular Mechanisms of Rhodopsin Retinitis Pigmentosa and the Efficacy of Pharmacological Rescue. J Mol Biol. 2010;395:1063–1078.

43. Hargrave PA. Rhodopsin structure, function, and topography the Friedenwald lecture. Invest Ophthalmol Vis Sci. 2001;42:3–9.

44. Parfitt DA, Aguila M, McCulley CH, Bevilacqua D, Mendes HF, Athanasiou D, et al. The heat-shock response co-inducer arimoclomol protects against retinal degeneration in

rhodopsin retinitis pigmentosa. Cell Death Dis. 2014;5:e1236.

45. Viringipurampeer IA, Metcalfe AL, Bashar AE, Sivak O, Yanai A, Mohammadi Z, et al. NLRP3 inflammasome activation drives bystander cone photoreceptor cell death in a P23H rhodopsin model of retinal degeneration. Hum Mol Genet. 2016;25:1501–1516.

46. LaVail MM. Kinetics of rod outer segment renewal in the developing mouse retina. J Cell Biol. 1973;58:650–661.

47. Luo D-G, Yau K-W. Rod Sensitivity of Neonatal Mouse and Rat. J Gen Physiol. 2005;126:263–269.

48. Chen Y, Jastrzebska B, Cao P, Zhang J, Wang B, Sun W, et al. Inherent instability of the retinitis pigmentosa P23H mutant opsin. J Biol Chem. 2014;289:9288–9303.

49. Pajares M, Cuadrado A, Rojo AI. Modulation of proteostasis by transcription factor NRF2 and impact in neurodegenerative diseases. Redox Biol. 2017;11:543–553.

50. Wang J, Saul A, Roon P, Smith SB. Activation of the molecular chaperone, sigma 1 receptor, preserves cone function in a murine model of inherited retinal degeneration. Proc Natl Acad Sci USA. 2016;113:E3764–E3772.

51. Inoue Y, Shimazawa M, Noda Y, Nagano R, Otsuka T, Kuse Y, et al. RS9, a novel Nrf2 activator, attenuates light-induced death of cells of photoreceptor cells and Müller glia cells. J Neurochem. 2017;141:750–765.

52. Ildefonso CJ, Jaime H, Brown EE, Iwata RL, Ahmed CM, Massengill MT, et al. Targeting the Nrf2 Signaling Pathway in the Retina With a Gene-Delivered Secretable and Cell-Penetrating Peptide. Invest Ophthalmol Vis Sci. 2016;57:372–386.

53. Byrne AM, Ruiz-Lopez AM, Roche SL, Moloney JN, Wyse -Jackson AC, Cotter TG, et al. The synthetic progestin norgestrel modulates Nrf2 signaling and acts as an antioxidant in a model of retinal degeneration. Redox Biol. 2016;10:128–139.

54. Nakagami Y, Hatano E, Inoue T, Yoshida K, Kondo M, Terasaki H. Cytoprotective Effects of a Novel Nrf2 Activator, RS9, in Rhodopsin Pro347Leu Rabbits. Curr Eye Res. 2016;41:1123–1126.

55. Chiang W-C, Hiramatsu N, Messah C, Kroeger H, Lin JH. Selective Activation of ATF6 and PERK Endoplasmic Reticulum Stress Signaling Pathways Prevent Mutant Rhodopsin Accumulation. Invest Ophthalmol Vis Sci. 2012;53:7159–7166.

56. Hammadi M, Oulidi A, Gackière F, Katsogiannou M, Slomianny C, Roudbaraki M, et al. Modulation of ER stress and apoptosis by endoplasmic reticulum calcium leak via translocon during unfolded protein response: involvement of GRP78. Faseb J. 2013;27:1600–1609.

57. Arroba AI, Wallace D, Mackey A, de la Rosa EJ, Cotter TG. IGF-I maintains calpastatin expression and attenuates apoptosis in several models of photoreceptor cell death. Eur J Neurosci. 2009;30:975–986.

58. Doonan F, Donovan M, Cotter TG. Caspase-independent photoreceptor apoptosis in mouse models of retinal degeneration. J Neurosci. 2003;23:5723–5731.

59. Kaur J, Mencl S, Sahaboglu A, Farinelli P, van Veen T, Zrenner E, et al. Calpain and PARP activation during photoreceptor cell death in P23H and S334ter rhodopsin mutant rats. PLoS One. 2011;6:e22181.

60. Paquet-Durand F, Sanges D, McCall J, Silva J, van Veen T, Marigo V, et al. Photoreceptor rescue and toxicity induced by different calpain inhibitors. J Neurochem. 2010;115:930–940.

61. Shimazawa M, Suemori S, Inokuchi Y, Matsunaga N, Nakajima Y, Oka T, et al. A novel calpain inhibitor, ((1S)-1-((((1S)-1-Benzyl-3-cyclopropylamino-2,3-di-oxopropyl)amino)carbonyl)-3-methylbutyl)carbamic acid 5-methoxy-3-oxapentyl ester

(SNJ-1945), reduces murine retinal cell death in vitro and in vivo. J Pharmacol Exp Ther. 2010;332:380–387.

62. Tzekov R, Stein L, Kaushal S. Protein misfolding and retinal degeneration. Cold Spring Harb Perspect Biol. 2011;3:a007492.

63. Sanges D, Marigo V. Cross-talk between two apoptotic pathways activated by endoplasmic reticulum stress: differential contribution of Caspase-12 and AIF. Apoptosis. 2006;11:1629–1641.

64. Petit A, Kawarai T, Paitel E, Sanjo N, Maj M, Scheid M, et al. Wild-type PINK1 prevents basal and induced neuronal apoptosis, a protective effect abrogated by Parkinson disease-related mutations. J Biol Chem. 2005;280:34025–34032.

Figure legends

Figure 1. Progression of photoreceptor demise and activation of calpains and AIF in *Rho*$^{P23H/+}$ retinas. (**a**) Percentages (±SD) of dying photoreceptors, based on TUNEL assay, at different ages of *Rho*$^{P23H/+}$ mice starting from post-natal day 8 (PN8) up to PN60, (N≥5). (**b**) Evaluation of intracellular Ca^{2+} in photoreceptor cells of *Rho*$^{+/+}$ and *Rho*$^{P23H/+}$ retinas. Intracellular Ca^{2+} was quantified by staining with Fluo-4 AM and flow cytometry analysis of photoreceptor cells (20,000 events analyzed). The median fluorescence intensity (MFI ±SD) from 4 different retinas is shown. *** P≥0.001 (**c**) Ratio of dying cells (TUNEL^{+}) (±SD) in which calpains are activated, based on the calpain activity assay (calpain^{+}), (N=4). No significant difference among the different time points could be detected by ANOVA test (P=0.059). (**d**) Total protein extracts from PN19 wild type (WT) and *Rho*$^{P23H/+}$ mutant mouse retinas were analyzed by immunoblots with an anti-αII-spectrin antibody shows an increase of the 145-150 kDa fragments resulting from calpain cleavage and of the 120 kDa fragment resulting from caspase cleavage. The immunoblot was normalized with anti-actin antibody (lower panel). MW: molecular weight markers are shown in kDa. (**e**) Immunoblotting of AIF in nuclear enriched protein extracts from PN19 WT and *Rho*$^{P23H/+}$ mutant mouse retinas. The immunoblot was normalized with anti-H3 histone antibody (lower panel). MW: molecular weight markers are shown in kDa. (**f**) Immunofluorescence labeling AIF (red) and TUNEL^{+} dying cells (green) in PN19 WT and *Rho*$^{P23H/+}$ mutant mouse retinas. Double-labeled cells (arrows and yellow in the merged image), i.e. dying cells with nuclear translocation of AIF, were observed in the mutant retina. Nuclei are stained in blue with DAPI. is: inner segment containing photoreceptor cytoplasm and mitochondria; onl: outer nuclear layer containing photoreceptor nuclei; inl; inner nuclear layer: gcl: ganglion cell layer. Scale bars: 20μm.

Figure 2. Activation of IRE1 and PERK in *Rho*$^{P23H/+}$ retinas. (**a**) Total protein extracts from PN19 and PN60 wild type (WT) and *Rho*$^{P23H/+}$ mutant mouse retinas were analyzed by immunoblots with an anti-phosphorylated IRE1 (P-IRE!), anti-phosphorylated PERK (P-PERK) and anti-phosphorylated eIF2α (P-eIF2α) antibodies. The immunoblots were normalized with anti-actin antibodies. (**b**) Immunofluorescence labeling of phosphorylated IRE1 or phosphorylated PERK (red) and TUNEL^{+} staining of dying cells (green) of PN19 and PN60 WT and *Rho*$^{P23H/+}$ mutant mouse retinas. Nuclei are stained in blue with DAPI. is: inner segment containing photoreceptor cytoplasm and ER; onl: outer nuclear layer containing photoreceptor nuclei. Scale bars: 20μm. (**c**) Total protein extracts from PN19 and PN60 WT and *Rho*$^{P23H/+}$ mutant mouse retinas were analyzed by immunoblots with anti-caspase 7 antibody. The immunoblot was normalized with anti-actin antibody (lower panel). (**d**) Immunoblotting of phosphorylated NRF2 in nuclear enriched protein extracts from PN19 and PN60 WT and *Rho*$^{P23H/+}$ mutant mouse retinas. The immunoblot was normalized with anti-H3 histone antibody (lower panel).

Figure 3. Treatments with PERK inhibitor. (**a**) Total protein extracts from PN19 *Rho*$^{P23H/+}$ mutant mouse retinas treated with vehicle (Mock) or with GSK2606414A (PERK inh) were analyzed by immunoblot with anti-phosphorylated eIF2α antibodies. The immunoblot was normalized with anti-eIF2α antibody (lower panel). (**b**) Percentages (±SD) of photoreceptors undergoing cell death (TUNEL^{+}) counted in the ONL of retinal sections passing through the optic nerve, (N=3). * P≥0.05 (**c**) Immunoblotting of phosphorylated NRF2 in nuclear enriched protein extracts from PN19 *Rho*$^{P23H/+}$ mutant mouse retinas treated with vehicle (Mock) or with GSK2606414A (PERK inh). The immunoblot was normalized with anti-H3 histone antibody (lower panel). (**d**) Total protein extracts from PN19 *Rho*$^{P23H/+}$ mutant mouse retinas treated with vehicle (Mock) or with GSK2606414A (PERK inh) were analyzed by immunoblot

with an anti-caspase 7 antibody. The immunoblot was normalized with anti-actin antibody (lower panel).

Figure 4. Inhibition of calpains and caspases in the *Rho*$^{P23H/+}$ retinas. *Rho*$^{P23H/+}$ mutant eyes were intravitreally injected with vehicle (Mock) or with PD150606 (calpain inhibitor) or with Z-VAD-FMK (caspase inhibitor) or with both PD150606 and Z-VAD-FMK at PN18 and analyzed at PN19. (**a**) Percentages (±SD) of photoreceptors that activated calpains counted in the ONL of retinal sections passing through the optic nerve, (N≥3). Student's t-test ** P≥0.01; *** P≥0.001. There was a significant effect of the treatments (ANOVA: F (3,23) = 151.3, P<0.0001). (**b**) Total protein extracts were analyzed by immunoblots with an anti-αII-spectrin antibody. The 145-150 kDa fragments resulting from calpain cleavage is indicated by an asterisk and of the 120 kDa fragment resulting from caspase cleavage by an arrow. The immunoblot was normalized with anti-actin antibody (lower panel). MW: molecular weight markers are shown in kDa. (**c**) Percentages (±SD) of photoreceptors undergoing cell death (TUNEL^{+}) counted in the ONL of retinal sections passing through the optic nerve, (N≥3). Student's t-test *** P≥0.001. There was a significant effect of the treatments (ANOVA: F (3,23) = 167.2, P<0.0001). (**d**) Total protein extracts were analyzed by immunoblots with an anti-caspase 7 antibody. The immunoblot was normalized with anti-actin antibody (lower panel). MW: molecular weight markers are shown in kDa.

Figure S1. Activation of calpains in *Rho*$^{P23H/+}$ retinas. (**a**) Controls for the specificity of the calpain assay. Retina cryosections from PN19 *Rho*$^{P23H/+}$ mutant mice were processed for the calpain activity assay either in the absence of t CMAC, t-BOC-Leu-Met substrate (No substrate) or after pretreatment of the crysection with the PD150606 calpain inhibitor (Calpain inh. pretreatment) to block calpain activity. No fluorescent signal could be detected

in the control experiments. (**b**) Retina cryosections from PN14, PN19, PN31 and PN60 wild type (WT) and *Rho*$^{P23H/+}$ mutant mice were exposed to a calpain substrate that becomes fluorescent (blue) upon cleavage by calpains. White dots in the outer nuclear layer (onl) containing photoreceptor cells identify cells activating calpains and were detected in mutant retinas but not in WT retinas. The same sections were assayed by TUNEL assay (red) to detect cells undergoing cell death. White dots in the outer nuclear layer (onl) containing photoreceptor cells identify dying cells and were detected in mutant retinas but not in WT retinas. The few PN60 photoreceptor cells undergoing cell death and activating calpains are indicated by arrows. Merged images of calpain activity staining and TUNEL are shown on the right-hand side. Scale bars: 50μm.

Figure S2. Validation of the specificity of antibodies used in western blotting experiments.

Antibodies used for western blotting to detect activation/phosphorylation of ER-stress sensors P-IRE1, P-PERK and P-eIF2α were validated on protein extracts from the NIH3T3 cell line treated with 2 μg/ml Tunicamycin, for 24 h as in Sanges et al [63]. Antibodies used for western blotting to detect activated/cleaved caspase-7 were validated on protein extracts from NIH3T3 cell line treated with 1 μM Staurosporine for 2 h, as in Petit et al [64]. Antibodies used for western blotting to detect nuclear translocation of NRF2 were validated on protein extracts from the NIH3T3 cell line treated with 5 μg/ml Tunicamycin for 30 min, as in Cullinan et al [37].

Figure S3. Entire membranes of western blotting experiments shown in Figures 1, 2, 3 and 4.

Figure S4. Cell death analyses on treated *Rho*$^{P23H/+}$ retinas. Sections from *Rho*$^{P23H/+}$ mutant PN19 retinas either treated with GSK2606414A (PERK inhibitor) or with PD150606 (calpain inhibitor) or Z-VAD-FMK (Caspase inhibitor) or with vehicle (mock) were analyzed by TUNEL assay (red). Nuclei were stained with DAPI (blue) and show all retinal cells. Red dots indicate dying cells.

Figure S5. Histological analysis of injected eyes. Examples of eyes stained with Hematoxylin and Eosin from not injected and intravitreally injected animals.

Figure 1

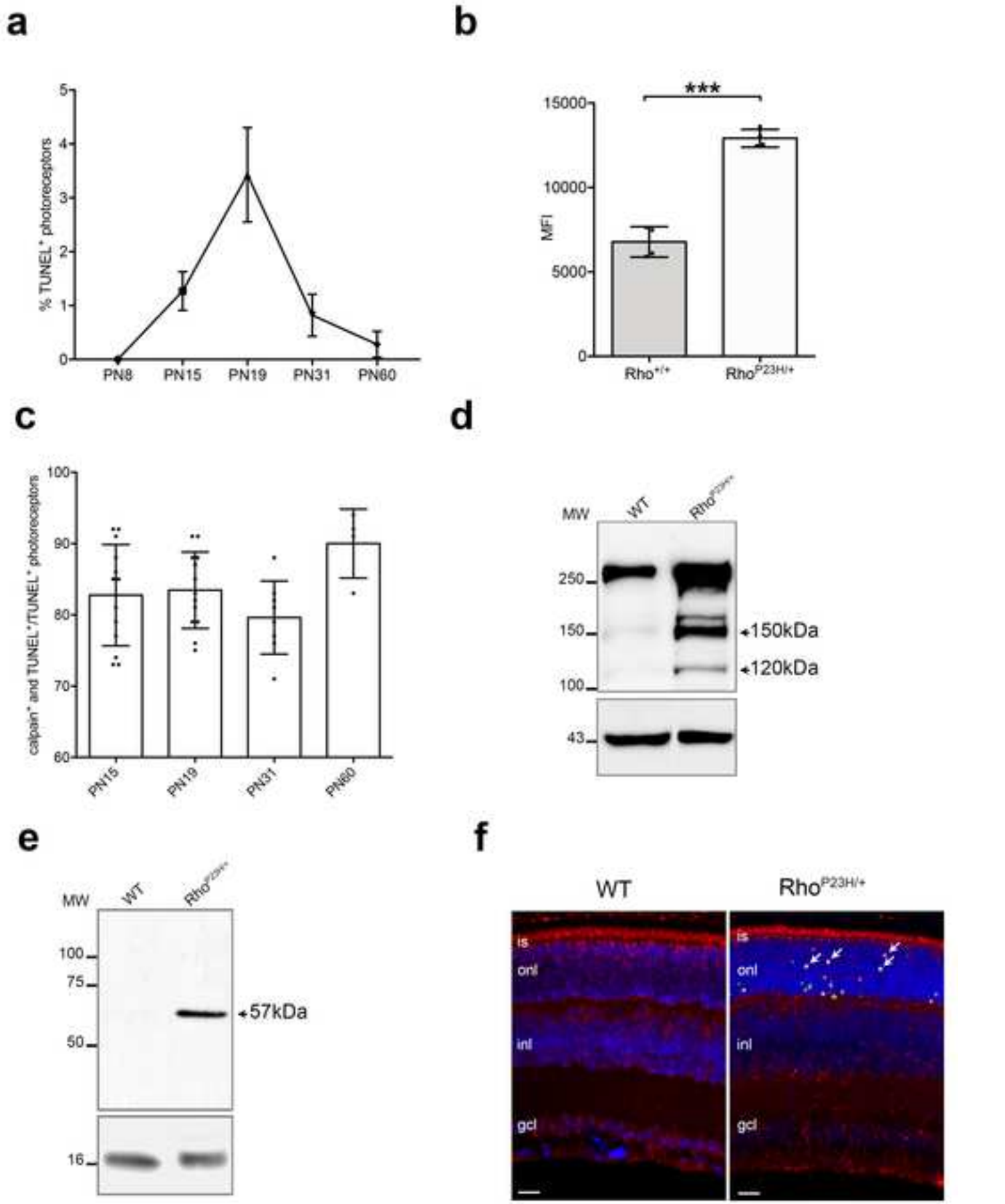

Figure 2

Click here to access/download;Figure;Figure 2.tif

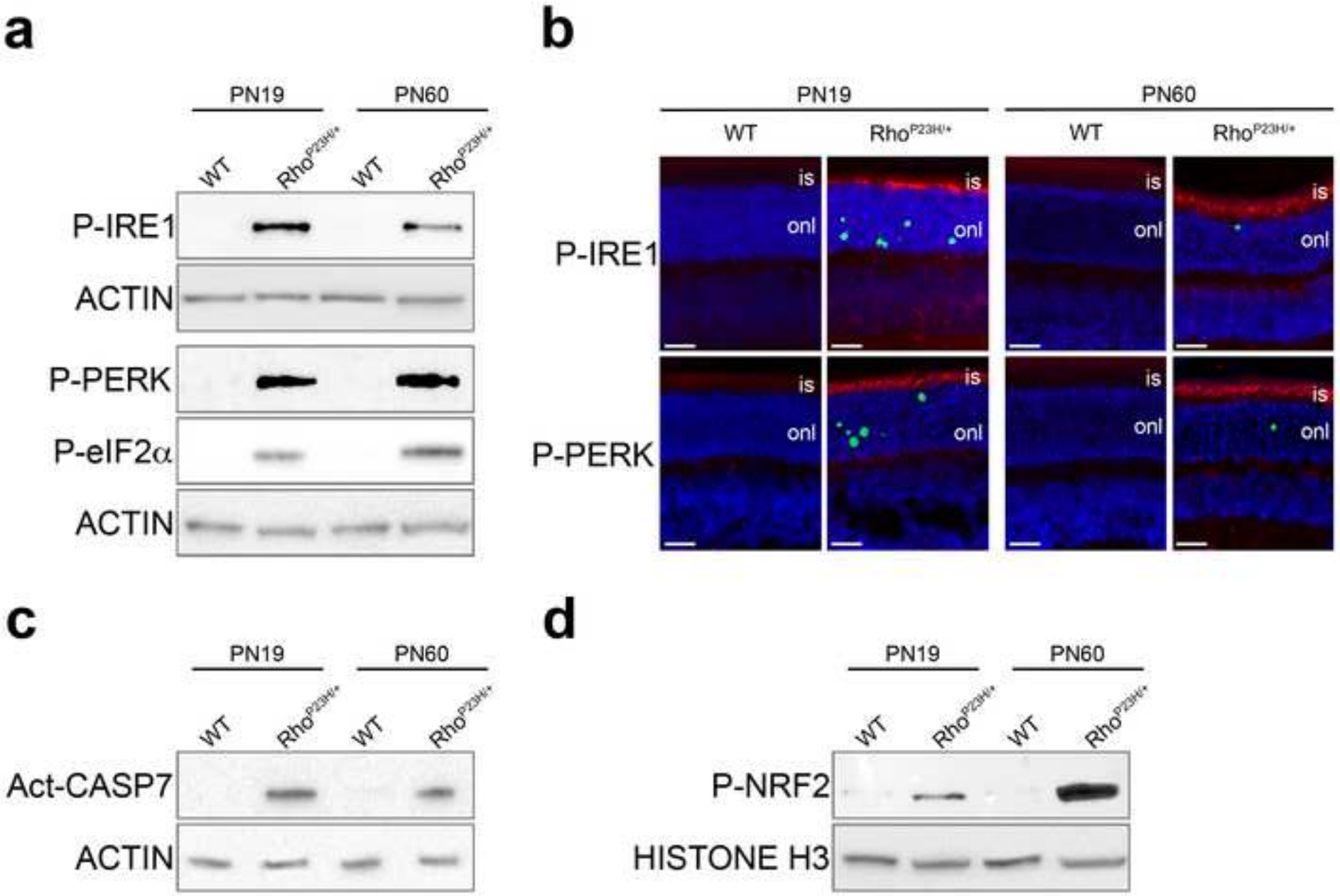

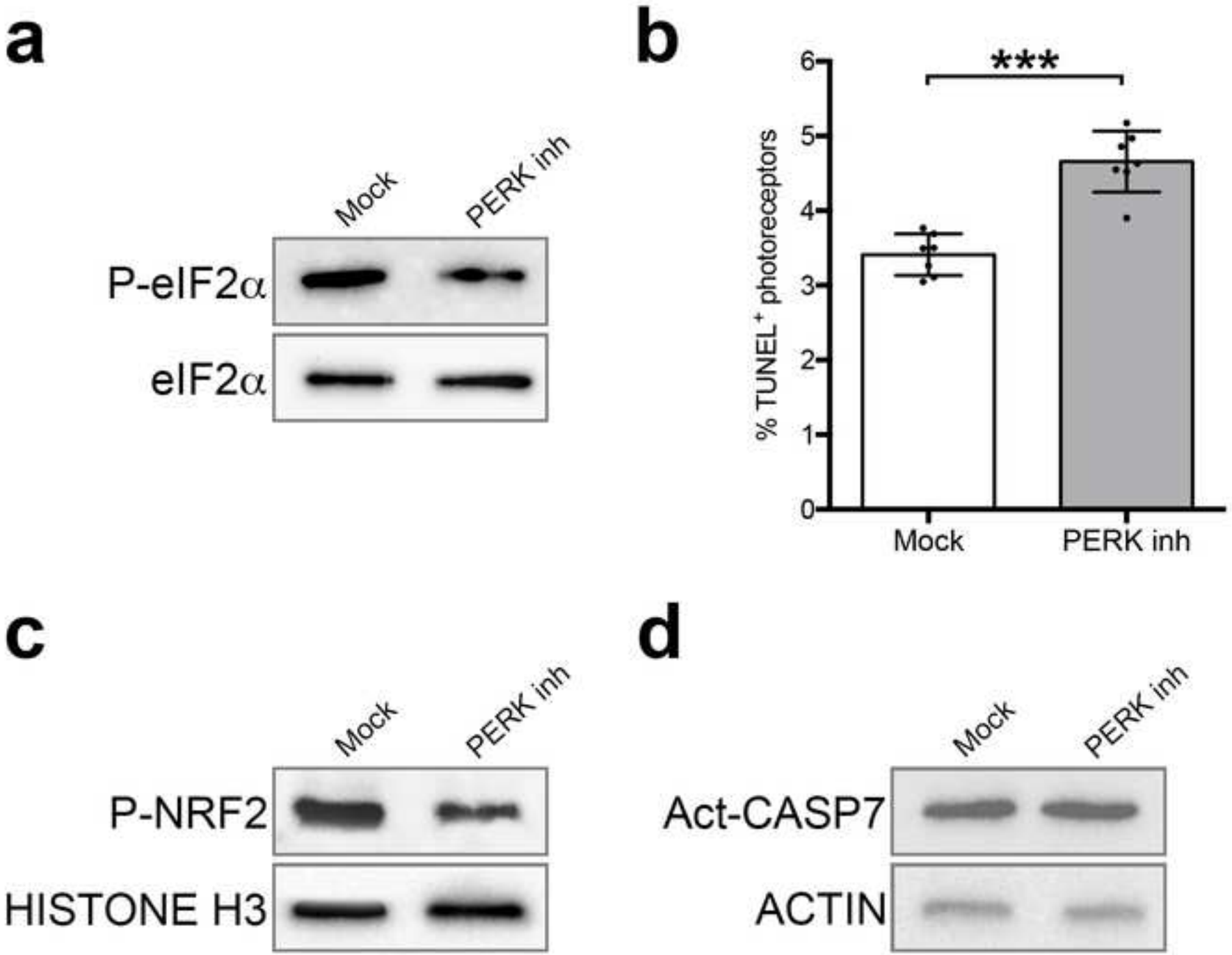

Figure 4

Click here to access/download;Figure;Figure 4.tif